Available online at www.sciencedirect.com
SCIENCE DIRECT®
Catalysis Today 89 (2004) 419–429
CATALYSIS TODAY
www.elsevier.com/locate/cattod

Novel utilization of mesoporous molecular sieves as supports of cobalt catalysts in Fischer–Tropsch synthesis

Yasuo Ohtsuka*, Yoshimoto Takahashi, Masato Noguchi, Takashi Arai, Satoshi Takasaki, Naoto Tsubouchi, Ye Wang[1]

Research Center for Sustainable Materials Engineering, Institute of Multidisciplinary Research for Advanced Materials, Tohoku University, Katahira, Aoba-ku, Sendai 980-8577, Japan

Received 15 August 2003; received in revised form 14 December 2003; accepted 10 January 2004

Abstract

Mesoporous molecular sieves (MCM-41 and SBA-15) with different pore diameters have been studied as supports of high loading of Co catalysts, and the performances in FT synthesis have been examined with a fixed bed stainless steel reactor at 2.0 MPa for the purpose of efficient production of C_{10}–C_{20} fraction as the main component of diesel fuel. The method of exchanging template ions in uncalcined MCM-41 with Co^{2+} ions is effective for holding 10–20% Co within the mesopores while keeping the structure regularity of MCM-41 to some extent, compared with the conventional impregnation method using calcined MCM-41. At 523 K, CO conversion and selectivity to C_{10}–C_{20} hydrocarbons are both higher at larger loading of 20% Co for the exchanged catalysts with pore diameters of 2.7–2.9 nm. When four kinds of 20% Co/SBA-15 with the diameters of 3.5–13 nm, prepared by the impregnation method using an ethanol solution of Co acetate, are used in FT synthesis at 523 K, the catalyst with the diameter of 8.3 nm shows the largest CO conversion, which is higher than those over MCM-41 supported Co catalysts. At a lower temperature of 503 K, however, the acetate-derived Co is almost inactive. In contrast, the use of Co nitrate alone or an equimolar mixture of the acetate and nitrate as Co precursor drastically enhances the reaction rate and consequently provides high space–time yield (260–270 g C/kg_{cat} h) of C_{10}–C_{20} hydrocarbons. The X-ray diffraction and temperature-programmed reduction measurements show that the dependency of the catalytic performance of 20% Co/SBA-15 on its precursor originates probably from the differences in not only the reducibility of the calcined catalyst but also the dispersion of metallic Co. Catalyst characterization after FT synthesis strongly suggests the high stability of the most effective Co/SBA-15 in the dispersion and reducibility of the oxide species and in the mesoporous structure.

Keywords: MCM-41; SBA-15; Cobalt catalysts; FT synthesis; Diesel fraction

1. Introduction

Fischer–Tropsch (FT) synthesis is a well-established process for the production of valuable long chain hydrocarbons from a mixture of CO and H_2, so-called syngas, derived from coal and natural gas. Stringent regulations on residual sulfur in diesel fuel and emission standards for particulate matters from diesel vehicles have recently roused renewed interest in FT synthesis, because it can produce super clean diesel oil fraction with high cetane number and without any sulfur and aromatic compounds using syngas from remote natural gas [1–7].

Supported Co-based catalysts have been widely used to achieve high yields of paraffinic hydrocarbons in FT synthesis [2,8–12]. Some papers published so far have focused on elucidating the roles of support and its porosity in reaction rate and product selectivity in the Co-catalyzed synthesis and suggested, for example, different degrees of metal dispersion and catalyst reduction, consequent different behaviors of CO and H_2 adsorption on Co particles, mass transport limitations for CO and hydrocarbons in catalyst pores, and pore filling by condensation of heavier hydrocarbons formed [9,13–17].

* Corresponding author. Tel.: +81-22-217-5653; fax: +81-22-217-5655.
E-mail address: ohtsukay@tagen.tohoku.ac.jp (Y. Ohtsuka).
[1] Present address: Department of Chemistry, Xiamen University, Xiamen 361005, PR China.

0920-5861/$ – see front matter © 2004 Elsevier B.V. All rights reserved.
doi:10.1016/j.cattod.2004.01.004

However, the effects of physical and chemical properties of supports on the performances of Co catalysts in FT synthesis remain still unclear [18]. The Co components are usually supported on SiO_2, Al_2O_3, and TiO_2 with microporous and mesoporous structures. Conventional mesoporous oxides are irregularly spaced and their pore sizes are broadly distributed. On the other hand, mesoporous molecular sieves recently developed, such as MCM-41 [19], FSM-16 [20] and SBA-15 [21], have well-defined periodic mesopores, consequently provide very narrow pore size distributions, and possess large pore volumes of 1–2 cm^3/g and high surface areas reaching 1000 m^2/g. The pore diameters can readily be controlled in the range of 2–30 nm by using various surfactants, some additives, and different synthetic conditions [22]. The utilization of such novel materials as supports of Co catalysts may make it possible to design new catalysts with higher productivity for C_{10}–C_{20} paraffin as the main component of diesel oil.

Thus, the present authors have been working on this topic [23–26]. Although a large number of papers have been published on synthesis, characterization and catalytic applications of MCM-41, FSM-16, SBA-15 and similar molecular sieves [22], only quite limited information on FT synthesis with them as catalyst supports, except for the present authors' work [23–26], has recently been provided [18,27–29]. When 15 mass% Co catalysts supported on hexagonal mesoporous silica (HMS) and MCM-41 with pore diameters of <3 nm were used in FT synthesis at 503 K and 2.0 MPa, for example, higher CO conversion and larger wax yield were observed with the HMS support [28]. The reason for this difference was not clear, though shorter channel and larger pore volume of the HMS were suggested to explain the difference. It has also been reported that, when the performances of 5–7 mass% Co catalysts loaded on MCM-41 and SBA-15 supports with different pore diameters of 2–9 nm are compared at low CO conversions of <5%, lower FT activity and higher CH_4 selectivity are observed at smaller catalyst pores due to lower reducibility of Co particles held within them [18].

Since the present authors' target is to achieve high space–time yield (STY) of C_{10}–C_{20} hydrocarbons as the main components of diesel fuel with mesoporous molecular sieves as catalyst supports, this article focuses on examining FT performances of Co catalysts at high loading of 20 mass% on MCM-41 and SBA-15 supports under the practical conditions of 503–523 K and 2.0 MPa, on extracting the key factors influencing CO conversion and C_{5+} selectivity from some observations obtained, and finally on improving the STY of the target product. Unique properties and structures of the molecular sieves, such as wide pores of >2 nm in diameter, large pore volumes of 1–2 cm^3/g, high surface areas reaching 1000 m^2/g, may enable ready diffusion of feed gas, avoid pore filling caused by condensation of heavier hydrocarbons, stabilize long-lived long chain radicals, and hold large amounts of Co species as nanoscale particles.

2. Experimental

2.1. Synthesis of mesoporous silica materials

The synthesis of MCM-41 was carried out according to the hydrothermal method reported elsewhere [19,30]. An acidic aqueous mixture of both sodium silicate as a SiO_2 source and $C_{16}H_{33}(CH_3)_3NBr$ as a template surfactant was first charged into a Teflon-made cylinder in a stainless autoclave and then held at 393 K during stirring. After the hydrothermal reaction for 96 h, as-synthesized MCM-41 was recovered by filtration, then dried at 313 K under vacuum and finally calcined in a stream of air at 823 K for 6 h to remove the template. The dried MCM-41 without calcination as well as the calcined MCM-41 was used as a catalyst support. The size of the calcined MCM-41 was in the range of 40–50 μm.

The preparation of SBA-15 was performed in a similar manner to that reported earlier [21]. An acidic aqueous mixture of tetraethyl orthosilicate as a SiO_2 source, a triblock copolymer, poly(ethylene oxide)–poly(propylene oxide)–poly(ethylene oxide), as a template, and trimethylbenzene (TMB) was first heated at 308 K for 24 h under ambient pressure and then subjected to post-synthesis treatment at 370 K. The ratio of TMB/copolymer and the treatment conditions were varied to produce SBA-15 supports with different pore diameters ranging from 3 to 12 nm [23]. Then, as-synthesized SBA-15 was separated by filtration, dried at room temperature under vacuum, and finally calcined under flowing air at 773 K for 6 h. The calcined SBA-15 with an average pore diameter of 8.6 nm was used as a support for Co catalyst, unless otherwise stated. The size of the calcined SBA-15 was roughly 50 μm.

2.2. Loading of cobalt components

Cobalt catalysts were loaded on the MCM-41 support in two different manners. One was the template ion exchange (TIE) method [31], in which an aqueous mixture of the uncalcined MCM-41 and $Co(CH_3COO)_2$ or $Co(NO_3)_2$, denoted as Co(A) or Co(N), respectively, was kept at 308 K for 24 h so that the template cations in the MCM-41 could be exchanged with Co^{2+} ions in Co(A) or Co(N). Since the ratio of the template cations to Co^{2+} ions is estimated to be 1.5 at Co loading of 10 mass%, the ion-exchangeable sites may be enough this case. However, the sites may be not sufficient for loading of 20 mass% Co. Part of Co^{2+} ions may be impregnated inside and/or outside the mesopores of the MCM-41 support.

Another was the conventional impregnation (IMP) method, in which the calcined MCM-41 was impregnated with an aqueous solution of Co(A) or Co(N) at ambient temperature. The exchanged and impregnated catalysts after removal of water were calcined again in the same way as mentioned above. The catalysts prepared by the TIE and IMP methods are denoted as Co-MCM-41 (TIE) and

Co/MCM-41 (IMP), respectively. Nominal loading of Co metal was 10 or 20 mass%. The amount of the actually loaded Co was not determined in this work.

When 10% Co and 1% Ru were co-loaded on the MCM-41 support, the two manners were used: both of Co and Ru cations were added simultaneously to the uncalcined MCM-41 by the TIE method, and the Co(A)-MCM-41 (TIE) was impregnated with an aqueous solution of $RuCl_3$.

Since the SBA-15 was prepared by using the triblock copolymer as a non-ionic surfactant, Co addition to the support was carried out at room temperature by the IMP method alone [23,26]. The effect of a solvent of Co precursor in the IMP process on the dispersion of the oxide species after air calcination was first examined, and an ethanol solution of Co(A), Co(N) or its equimolar mixture (denoted as Co(A + N)) was then selected. After removal of ethanol, the resulting sample was air-calcined again at 773 K as mentioned above. The SBA-15 supported catalyst is represented as Co/SBA-15. Loading of Co metal in it is expressed in *x* and *y* mass% of Co(*x*A + *y*N); for example, Co(10A + 10N) indicates 10 mass% Co from $Co(CH_3COO)_2$ and 10 mass% Co from $Co(NO_3)_2$, and Co(20N) does 20 mass% Co from $Co(NO_3)_2$ alone. The same abbreviations are employed to express Co catalysts supported on MCM-41, such as Co(10A)/MCM-41 and Co(10N)-MCM-41.

2.3. Characterization of supports and catalysts

The N_2 adsorption measurements of these supports and catalysts were made at 77 K. The specific surface area was estimated by the BET method. The pore size distribution and pore volume was determined by the BJH method. Average pore diameters of SBA-15 supports and Co/SBA-15 catalysts were calculated by using total volume and surface area of the mesopores on the assumption that they are cylindrical [21].

The X-ray diffraction (XRD) analysis before and after FT synthesis was carried out with a conventional powder diffractometer using Ni-filtered Cu Kα radiation (40 kV, 30 mA). The average crystalline size of Co_3O_4 identified by the XRD was calculated by the Debye–Scherrer method. The small angle X-ray scattering (SAXS) measurements of some Co/SBA-15 catalysts were performed using Cu Kα radiation (40 kV, 80 mA).

In order to examine the reducibility of Co species in calcined catalysts, the temperature programmed reduction (TPR) measurements were made by heating at a rate of 10 K/min up to 1273 K in a stream of 67.5 vol.% H_2 diluted with Ar, and the changes in H_2 concentration were on line monitored with a gas chromatograph with a thermal conductivity detector.

2.4. FT synthesis and product analysis

The reaction run was performed with a stainless fixed-bed reactor. The apparatus and procedure have been described in detail elsewhere [26] and is thus simply explained below. After the catalyst sample charged into the reactor was pretreated with atmospheric H_2 at 673 K for 12 h, the H_2 was replaced at 373 K with a pressurized mixture of H_2 and CO, and finally the reactor was heated up to reaction temperature. The temperature could be controlled and measured with a thermocouple inserted into the catalyst bed. After the FT run, the reactor was quenched to room temperature. Catalyst weight (*W*), *W*/*F* (*F*, feed rate), H_2/CO ratio, reaction temperature and pressure were 0.50 g, 4.0 g h/mol, 2.0, 503 or 523 K, and 2.0 MPa, respectively, unless otherwise stated.

Liquid products formed were recovered with three kinds of traps, and C_6–C_{28} hydrocarbons in them were determined with a capillary GC–MS. Lower hydrocarbons (C_1–C_5) in the effluent after recovery of the liquid products were on line analyzed with a high-speed micro-GC [26]. Waxy materials remaining in the catalyst recovered after the FT run were also determined by the conventional elemental analyzer.

3. Results and discussion

3.1. Properties of Co catalysts supported on MCM-41

The XRD profiles for the fresh catalysts are shown in Fig. 1, where those for MCM-41 supports before and after air calcination are also illustrated for comparison. The

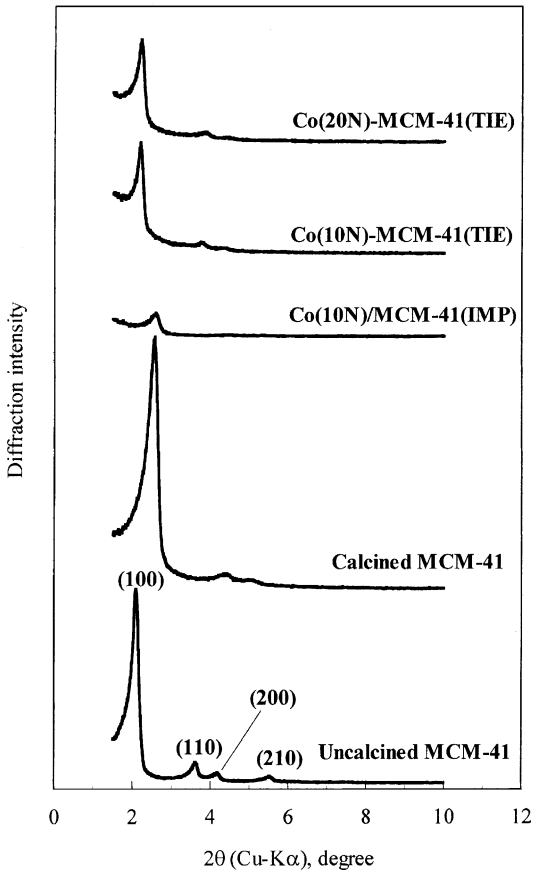

Fig. 1. XRD profiles for MCM-41 supports and Co catalysts.

Table 1
Properties of MCM-41 supported Co catalysts

Support and catalyst[a]	Co loading (mass%)	Pore properties		S_{BET}[b] (m^2/g)	$D(Co_3O_4)$[c] (nm)
		Diameter (nm)	Volume (cm^3/g)		
MCM-41	0	2.2	0.75	1060	–
Co(N)/MCM-41 (IMP)	10	2.2	0.47	740	8.6
Co(A)/MCM-41 (IMP)	10	2.1	0.42	710	n.d.[d]
Co(N)-MCM-41 (TIE)	10	2.9	1.2	840	n.d.[d]
Co(A)-MCM-41 (TIE)	10	2.7	1.1	890	n.d.[d]
Co(N)-MCM-41 (TIE)	20	2.9	0.98	780	13
Co(A)-MCM-41 (TIE)	20	2.9	0.95	770	n.d.[d]

[a] Co(N), Co nitrate; Co(A), Co acetate; IMP, impregnation; TIE, template ion exchange.
[b] Surface area measured by the BET method.
[c] Average crystalline size of Co_3O_4 estimated by the Debye–Scherrer method.
[d] No species detectable by XRD.

uncalcined MCM-41 provided distinct four diffraction lines due to SiO_2 (1 0 0), (1 1 0), (2 0 0), and (2 1 0) planes, showing hexagonal structures, as reported earlier [30]. After air calcination at 823 K, the diffraction angles (2θ) of the (1 0 0), (1 1 0) and (2 0 0) lines shifted slightly to larger values.

When the XRD results were compared with the calcined MCM-41 and the Co(10N)/MCM-41 (IMP) catalyst, the intensity of SiO_2 (1 0 0) was much lower with the latter, and any other lines were not observed, showing the considerable lowering in the structure regularity of the catalyst. With the Co(10N)-MCM-41 (TIE), on the other hand, the position of the (1 0 0) peak was equal to that for the uncalcined MCM-41, and the (1 1 0) and (2 0 0) planes were still present. Although the intensity of the (1 0 0) line was decreased by Co addition, it was much larger than that for the Co(10N)/MCM-41 (IMP). When Co loading in the Co-MCM-41 (TIE) was increased from 10 to 20%, the XRD profile was almost unchanged. The use of Co(A) in place of Co(N) had almost no effect on the XRD results. It is evident that the hexagonal structures of the uncalcined MCM-41 are still retained to some extent even by adding 10–20% Co by the TIE method.

As expected, all of the Co catalysts used as well as the MCM-41 support showed very narrow pore size distribution [24]. The pore properties and BET surface areas are summarized in Table 1. The pore diameter, pore volume and surface area of the calcined support were 2.2 nm, 0.75 cm^3/g and 1060 m^2/g, respectively. With the Co catalysts, these values were dependent on the method of catalyst addition and loading of Co metal but almost independent of the kind of its precursor. The pore diameters of Co(10N)/and Co(10A)/MCM-41 (IMP) catalysts were 2.1–2.2 nm, which were nearly equal to that of the support but lower than those (2.7–2.9 nm) of Co(10N)- and Co(10A)-MCM-41 (TIE) catalysts. When Co loading was increased to 20% in the latter case, the diameter was almost unchanged. Such differences in the diameter among these catalysts corresponded well to the changes in the diffraction angle of the (1 0 0) line mentioned above.

As shown in Table 1, the pore volumes of the Co(10N)/and Co(10A)/MCM-41 (IMP) decreased to about 60% of that of the MCM-41 support. This decrease is reasonable, because Co particles were held inside the mesopores. In contrast, the volume was rather larger with the Co-MCM-41 (TIE), regardless of both the kind of Co precursor and the catalyst loading, than with the support alone. The reason is not clear but may be related with the larger pore diameters (Table 1) of the Co-MCM-41 (TIE). In the TIE process, part of ion pairs, in other words, Co cations and the counter anions, might be inserted into the weak ionic bonds between the template cations in the uncalcined MCM-41 and the silicate anions, and such insertions could help protect the support pores from collapsing upon calcination, which results in the larger pore diameters and higher pore volumes, compared with those of the support alone. This speculation may be supported by the XRD results (Fig. 1) that the diffraction angles of the (1 0 0) lines observed with Co(10N)- and Co(20N)-Co-MCM-41 (TIE) catalysts are the same as that with the uncalcined MCM-41.

Fig. 2 shows the XRD profiles at 2θ (Cu Kα) of 20–80° to clarify crystalline states of Co catalysts at loading of 10%. The use of Co(A) provided no significant XRD peaks attributable to Co species, irrespective of the method of catalyst addition. When Co(N) was used in place of Co(A), the weak diffraction lines of Co_3O_4 were observed for the Co(10N) (IMP), whereas any XRD signals of this species could not be detected for the Co(10N) (TIE). As shown in Table 1, the average crystalline size of Co_3O_4 observed with the former catalyst was estimated to be 8.6 nm. Table 1 also shows the XRD results for 20% Co catalysts prepared by the TIE method. Although the diffraction lines of Co_3O_4 with the average size of 13 nm were observed for the Co(20N), no XRD peaks of the oxide were detectable with the Co(20A). These observations point out that Co species are more highly dispersed in the TIE method than in the IMP one, and that the crystallization upon calcination proceeds more readily with the Co(N) than with the Co(A). The average sizes of Co_3O_4 crys-

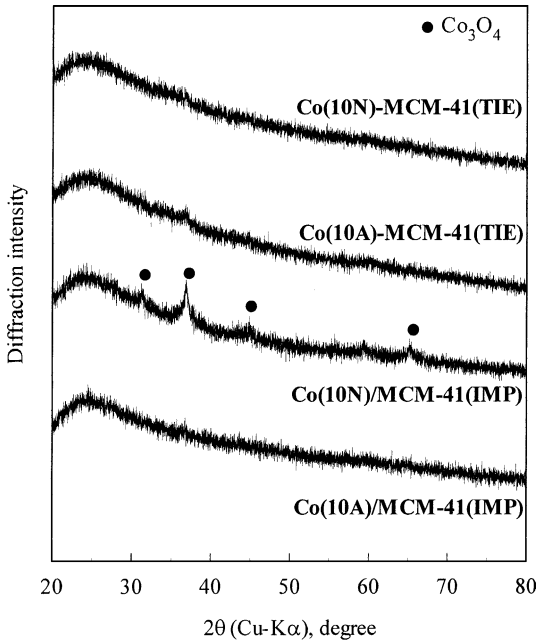

Fig. 2. XRD profiles for MCM-41 supported Co catalysts after air calcination.

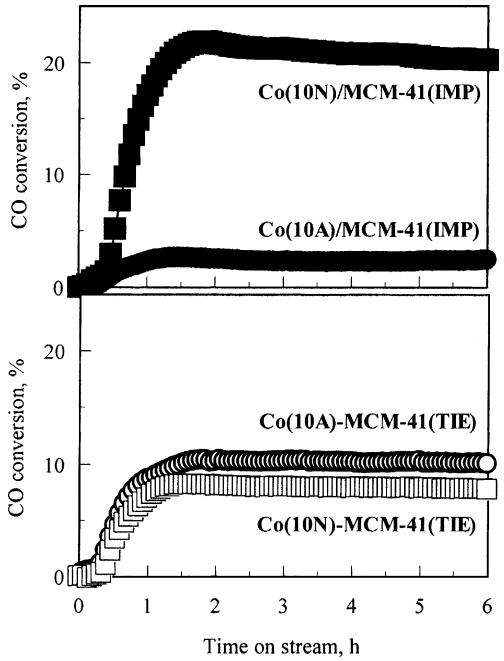

Fig. 3. CO conversion during FT synthesis with different Co catalysts at 523 K.

tallites detected were larger than the corresponding pore diameters (2.2–2.9 nm), showing that some of Co_3O_4 are held outside the mesopores. It is probable that the Co particles can readily agglomerate to be crystallized due to weak interactions with the support, compared with those inside the pores. The crystallized Co is detectable by the XRD.

The observations described above suggest that the TIE method utilizing the uncalcined MCM-41 works more efficiently for holding large amounts of 10–20% Co within the mesopores of the support while keeping the structure regularity to some extent, compared with the impregnation method using the calcined MCM-41. Therefore the Co-MCM-41 (TIE) catalysts are mainly used in FT synthesis.

3.2. Performances of MCM-41 supported Co catalysts in FT synthesis

Fig. 3 compares the activity of four kinds of 10% Co catalysts in FT synthesis at 523 K. CO conversion increased gradually with increasing time on stream, and it was steady after about 1.5 h, regardless of the kind of the catalyst. The conversion over the Co-MCM-41 (TIE) was almost the same between the Co(10N) and the Co(10A), whereas the activity of the Co/MCM-41 (IMP) was much higher with the Co(10N) than with the Co(10A). As a result, the Co(10N)/MCM-41 (IMP) showed the largest conversion of 20% among the four catalysts.

The catalytic performances are summarized in Table 2, where CO conversion after 6 h reaction is provided, and

Table 2
Performances of MCM-41 supported Co catalysts in FT synthesis at 523 K

Catalyst[a]	Co conversion[b] (%)	Product selectivity[c] (C mol%)				α[d]
		C_1–C_4	C_5–C_9	C_{10}–C_{20}	C_{21}+[e]	
Co(10N)/MCM-41 (IMP)	20	47	25	21	7	0.70
Co(10A)/MCM-41 (IMP)	2.4	n.a.	n.a.	n.a.	n.a.	n.a
Co(10N)-MCM-41 (TIE)	7.7	42	32	18	8	0.73
Co(10A)-MCM-41 (TIE)	10	37	30	24	10	0.70
Co(20N)-MCM-41 (TIE)	50	34	33	27	6	0.71
Co(20A)-MCM-41 (TIE)	33	34	31	31	4	0.75

[a] Keys as in Table 1.
[b] CO conversion after 6 h reaction.
[c] Average value during 6 h reaction.
[d] Chain growth probability.
[e] Including waxy materials remaining in catalyst after reaction.

product selectivity is expressed as an average value during 6 h reaction. The amount of CO_2 was always negligible small. With product distribution among three kinds of 10% Co catalysts, selectivity to lower hydrocarbons (C_1–C_4) or diesel oil fraction (C_{10}–C_{20}) was smaller or larger with the Co(10A)-MCM-41 (TIE), respectively, CH_4 selectivity being 19–20 C mol%, irrespective of the kind of catalyst. When metal loading in the Co-MCM-41 (TIE) catalyst was increased from 10 to 20%, CO conversion increased remarkably in both cases, but the increment was higher for the Co(20N) than for the Co(20A); the conversion over the former catalyst reached 50%, which was 6.5 times that at 10% Co. Interestingly, the increase in Co loading from 10 to 20% lead to higher selectivity to C_{10}–C_{20} fraction, irrespective of the type of Co precursor, and the values were 27–31 C mol%, which were 1.3–1.5 times those at 10% Co. CH_4 selectivity was almost independent of Co loading. It is evident that Co loading is one of the key factors determining the performance of the Co-MCM-41 (TIE) catalyst in the production of diesel oil fraction.

As indicated by comparing the results in Tables 1 and 2, the Co(10N)/MCM-41 (IMP) and Co(20N)-MCM-41 (TIE), which both provided the XRD peaks of Co_3O_4 after air calcination, showed the highest CO conversions among the corresponding 10 or 20% Co catalysts. These observations suggest that the extent of crystallization of Co species is related closely to the catalytic activity. It has been reported that, when Co(10N) or Co(10A) is impregnated with a conventional SiO_2 support, the Co(10N) is more readily crystallized and reduced during air calcination and subsequent H_2 reduction, respectively, and that the Co(10N) is more active in FT synthesis [32]. We have also shown that the crystallization and reduction of 20% Co/SBA-15 proceeds to a larger extent with the Co(20N) than with the Co(20A), and the former exhibits higher FT activity [26]. These results point out that the high degree of Co crystallization means weak interactions with catalyst support and thus lead to the ready reduction to metallic Co, which catalyzes FT synthesis effectively.

Since the coexistence of a small amount of Ru enhanced the reduction of Co oxides on conventional SiO_2 supports and thus increased the rate of FT synthesis [33,34], two kinds of Co(10A) catalysts including 1% Ru were prepared by the IMP and TIE methods and then subjected to the FT run. No significant effect of the Ru addition on CO conversion at 523 K was observed with the two catalysts. The reason is not clear, but interactions between Co(A) and SiOH groups in the MCM-41 support might be too strong for Co species to be reduced.

3.3. Properties of Co catalysts supported on SBA-15

As mentioned above, the method of Co addition and the kind of its precursor remarkably affected the crystallization of the oxide species formed upon calcination. It has been accepted that the formation of small crystallites of Co oxides leads to high dispersion of metallic Co, which results in the large catalytic activity for FT synthesis [9,17,26,32]. The effects of Co precursor and solvent used in the impregnation process on the average crystalline size of Co_3O_4 were thus examined using the SBA-15 support with average pore diameter (denoted as D_{av} thereafter) of 3.5 nm and pore volume of 0.6 cm^3/g. The results are summarized in Table 3. When Co(N) was used at loading of 10%, the XRD peaks of Co_3O_4 appeared with all of three solvents examined, whereas the average size decreased in the sequence of water > acetone > ethanol. The decrease in Co loading from 10 to 5% with an ethanol solution of Co(N) provided no diffraction lines of any oxide species, which are probably too fine to be detected by XRD. The use of Co(A) in place of Co(N) showed the absence of any XRD signals of Co oxides as well, even at higher loading of 20% Co. This observation can be explained by the formation of amorphous Co silicates and surface oxide species, as shown later.

Table 3
Crystalline states after air calcination of Co/SBA-15 catalysts prepared under different conditions

Co precursor[a]	Solvent	Co loading (mass%)	$D(Co_3O_4)$[b] (nm)
Co(N)	Water	10	19
Co(N)	Acetone	10	12
Co(N)	Ethanol	5	n.d.[c]
Co(N)	Ethanol	10	9.5
Co(A)	Ethanol	10	n.d.[c]
Co(A)	Ethanol	20	n.d.[c]

[a] SBA-15 support with average pore diameter of 3.5 nm: Co(N), Co nitrate; Co(A), Co acetate.
[b] Average crystalline size of Co_3O_4.
[c] No species detectable by XRD.

According to the results in Table 3, all of Co/SBA-15 catalysts for FT synthesis were prepared by an ethanol solution of Co(N) or Co(A). Fig. 4 shows typical examples of pore size distribution for four kinds of Co(20A)/SBA-15 catalysts with different D_{av}. Each catalyst provided a single peak at the pore diameter of 3.6, 5.5, 8.4, or 13.8 nm. As the diameter of the peak position was larger, the peak shape was asymmetric and broad, as observed for SBA-15 supports with different D_{av} [23]. The SAXS measurements showed that a strong (1 0 0) line was detectable for the Co(20A) catalyst with D_{av} of 5.4 nm, whereas no scattering peaks were observed with the Co(20A) with the largest D_{av} of 13 nm, suggesting the formation of less organized pore structures.

The properties of different Co catalysts are summarized in Table 4, where Fe(20N) catalyst prepared from an ethanol solution of $Fe(NO_3)_3$ is included as a reference. With Co(20A)/SBA-15 catalysts, the pore volume increased with increasing D_{av}, whereas the surface area seemed to be the largest at D_{av} of 5.4 nm. When the XRD results were compared among four kinds of Co catalysts with almost the same D_{av} of 8.2–8.6 nm, all of the Co(10A + 10N), Co(10N), and Co(20N) catalysts including Co(N) provided the diffraction lines of Co_3O_4, and the average crystalline

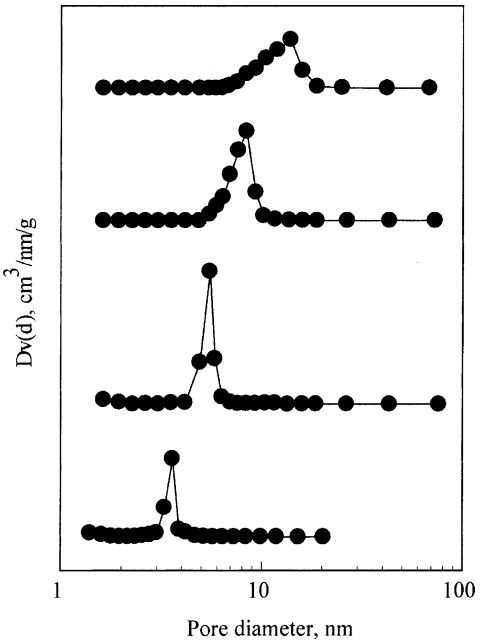

Fig. 4. Pore size distribution for Co(20A)/SBA-15 catalysts with different pore diameters.

size was estimated to be 9.1–20 nm, as seen in Table 4. It thus tended to be larger in the sequence of Co(10A+10N) < Co(10N) < Co(20N). The slightly larger sizes than the corresponding D_{av} suggest that part of the Co_3O_4 particles may be present outside of the catalyst pores. Since it has been shown that the pore volume and surface area of the SBA-15 support lower remarkably by Co addition [23,26], however, it is reasonable to see that most of Co particles can be held inside the mesopores. The crystallization of the Co present outside the pores would rather readily proceed due to weak interactions with surface SiOH groups of the support. The crystallized Co can be detected by the XRD and may readily be reduced with H_2 to form large particles of metallic Co. Table 4 also reveals that no XRD peaks attributable to any Fe oxides are detectable with the Fe(20N) catalyst.

Table 4
Properties of Co/SBA-15 and Fe/SBA-15 catalysts with different pore diameters

Catalyst[a]	D_{av}[b] (nm)	V_p[b] (cm^3/g)	S_{BET}[b] (m^2/g)	D_{crys}[c] (nm)
Co(20A)	3.5	0.31	360	n.d.[d]
Co(20A)	5.4	0.69	530	n.d.[d]
Co(20A)	8.2	1.2	460	n.d.[d]
Co(20A)	13	1.7	450	n.d.[d]
Co(10A + 10N)[e]	8.2	1.4	530	9.1
Co(10N)[e]	8.6	1.6	720	12
Co(20N)[e]	8.5	1.3	590	20
Fe(20N)	8.3	1.2	650	n.d.[d]

[a] Co(A), Co acetate; Co(N), Co nitrate; C(A + N), a mixture of Co(A) and Co(N).
[b] D_{av}, average pore diameter; V_p, pore volume; S_{BET}, BET surface area.
[c] Average crystalline size of Co_3O_4 or Fe_2O_3 for Co or Fe catalyst, respectively.
[d] No metal oxides detectable by XRD.
[e] Ref. [26].

3.4. Performances of SBA-15 supported Co catalysts in FT synthesis

The results for FT runs at 503 and 523 K are summarized in Table 5. When the effect of the average pore diameter of Co(20A)/SBA-15 catalyst on the FT performance at 523 K was examined, the catalyst with the diameter of 8.2 nm showed the largest CO conversion of 72% after 6 h reaction. The similar dependency has been reported in FT synthesis with 20% Co(N) catalysts on conventional SiO_2 supports with mean pore diameters of 2–15 nm; the highest CO conversion at 493 K is observed with the support with the moderate diameter of 10 nm [17]. Narrow pores of not only conventional but also periodic mesoporous SiO_2 supports, compared with wide pores, lead to formation of smaller Co oxides, which were more difficult to reduce probably due to stronger interactions between metal and support than the larger particles, and such interactions resulted in higher dispersion of metallic Co reduced [17,18]. The highest activity of the Co(20A) catalyst with D_{av} of 8.2 nm may thus be explained by the interplay between catalyst reducibility and dispersion.

Table 5 also reveals that the chain growth probability (α) observed with the most active Co(20A) catalyst at 523 K is as low as 0.72, which means that CH_4 and lower paraffin (C_2–C_4) are the main products, whereas selectivity to C_{10}–C_{20} fraction is only 8 C mol%.

On the basis of the above-mentioned observations, the SBA-15 support with D_{av} of about 8.5 nm is used in the following FT runs, and the temperature is decreased from 523 to 503 K to suppress CH_4 formation. The results are also shown in Table 5. The amount of CO_2 was always negligible small, and CH_4 selectivity was almost the same (15–17 C mol%), irrespective of the kind of catalyst. As seen in Table 5, CO conversion at 503 K was only 1% with the Co(20A) with D_{av} of 8.3 nm [26], which was nearly equal to that (8.2 nm) of the most active catalyst at 523 K. In contrast, CO conversions over the Co(10A + 10N) and Co(20N) catalysts with the respective D_{av} of 8.2 and 8.5 were as large as 84–89% [26]. Compared with these catalysts, the Co(10N) and Fe(20N) were much less active, as shown in Table 5. Since CO conversion over the Co(10A + 10N) remarkably exceeds the sum of those observed with the Co(20A) and Co(10N), it is evident that the synergistic effect exists with the catalytic activity of the Co(10A + 10N) [26].

To clarify the activity difference between the Co(20A) and Co(20N) catalysts, the TPR measurements were carried out. The results are illustrated in Fig. 5. These fresh catalysts after air calcination showed the quite distinct profiles [26]; the Co(20A) had only a broad peak at 900–1200 K (Fig. 5A), but contrarily the Co(20N) provided the main and shoulder peaks at lower temperatures of $\leq$800 K (Fig. 5B). The H_2 consumption at $\geq$900 K and $\leq$800 K may be identified to

Table 5
CO conversion, selectivity to C_{10}–C_{20} fraction and chain growth probability over Co/SBA-15 and Fe/SBA-15 catalysts with different pore diameters

Catalyst[a]	Temperature (K)	CO conversion[b] (%)	C_{10}–C_{20}[c] (C mol%)	α[d]
Co(20A) (3.5)	523	14	13	0.69
Co(20A) (5.4)	523	5.6	n.a.	n.a.
Co(20A) (8.2)	523	72	8	0.72
Co(20A) (13)	523	6.8	n.a.	n.a.
Co(20A) (8.3)[e]	503	1.0	n.a.	n.a.
Co(10A + 10N) (8.2)[e]	503	84	32	0.93
Co(10N) (8.6)[e]	503	20	30	0.87
Co(20N) (8.5)[e]	503	89	30	0.92
Fe(20N) (8.3)	503	14	7	0.84

[a] Keys as in Table 4; values in parentheses denote average pore diameters.
[b] CO conversion after 6 h reaction.
[c] Average selectivity during 6 h reaction.
[d] Chain growth probability.
[e] Ref. [26].

the reduction of Co silicates and/or surface CoO_x species to metallic Co and of Co_3O_4 to CoO and subsequently Co, respectively [35–38]. The silicate species in the Co(20A), if any, are not crystallized and/or present at the outermost layer, because no diffraction lines of any Co species were detectable with the fresh Co(20A), as indicated in Table 4. Table 4 also confirmed the presence of Co_3O_4 as the bulk phase of the fresh Co(20N).

When the Co(20N) charged into a quartz reactor in the TPR apparatus was first pretreated with H_2 at 673 K for 12 h, in other words, in the same manner as that for the H_2 pretreatment before the FT run, and then subjected to the TPR measurement, no significant H_2 consumption took place up to 800 K, as shown in Fig. 5C. This strongly suggests almost complete reduction of Co_3O_4 in the Co(20N) to metallic Co. On the other hand, the Co species in the Co(20A) must remain unreduced even after the H_2 pretreatment. It is probable that such a distinct reducibility to metallic Co observed with the Co(20A) and Co(20N) catalysts leads to the activity difference between the two.

Although the Co(20A)/SBA-15 was almost inactive at 503 K, it exhibited high activity when the temperature was raised to 523 K (Table 5). Since the Co(20A) was strongly resistant to the H_2 reduction at 673 K before the FT run (Fig. 5A), the Co species may be reduced to metallic Co with the CO in feed gas and consequently active.

As shown in Table 5, selectivity to C_{10}–C_{20} hydrocarbons and chain growth probability (α) were both much larger with the Co(20N) and Co(10A + 10N) at 503 K than with the Co(20A) at 523 K. The former two catalysts provided the selectivity of 30–32 C mol% and α of 0.92–0.93 at 503 K [26]. Fig. 6 summarizes space–time yield of C_{10}–C_{20} fraction and CO conversion against catalyst composition. The

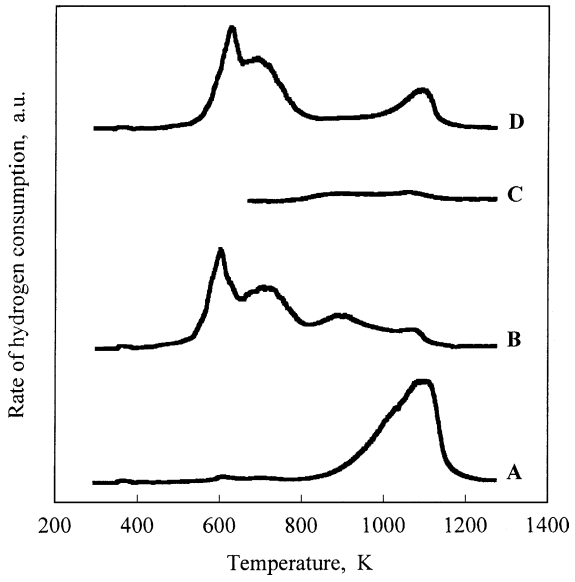

Fig. 5. TPR profiles for different Co/SBA-15 catalysts: (A) fresh Co(20A) catalyst after air calcination; (B) fresh Co(20N) catalyst after calcination; (C) fresh Co(20N) catalyst after H_2 reduction at 673 K; (D) used Co(20N) catalyst after re-calcination.

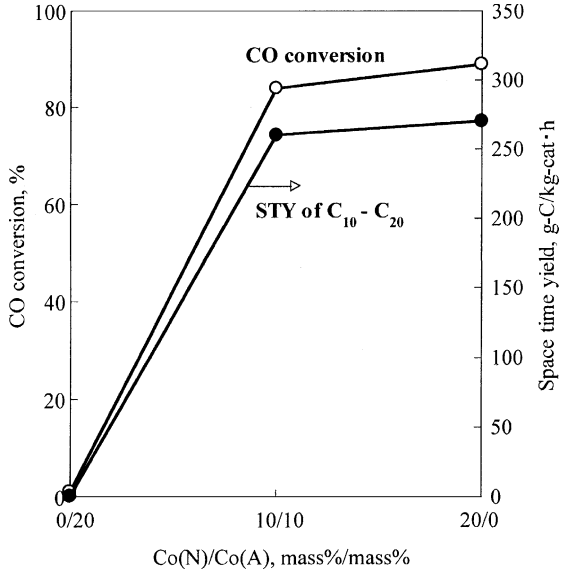

Fig. 6. Performances of Co/SBA-15 catalysts in FT synthesis at 503 K.

Table 6
Comparison in space–time yield of C_{10}–C_{20} hydrocarbons among different Co catalysts supported on conventional SiO_2 and mesoporous molecular sieves

Catalyst properties[a]				FT synthesis				Remarks[d]
Support	D_{av} (nm)	V_p (cm^3/g)	Co loading (mass%)	T (K)	P (MPa)	W/F[b] (g h/mol)	STY (g C/kg_{cat} h)[c]	
SiO_2	8.7	1.2	20, 25	503	1.0	5.0	90, 100	Slurry [32]
SiO_2	10	2.0	20	493	1.5	27	40	Slurry [17]
SiO_2	16	1.2	20[e]	493	1.0	5.0	210	Gas [39]
HMS[f]	2.8	0.4	15	513	2.0	24	60	Gas [28]
MPAS[g]	2.5	0.6	20[g]	503	1.0	10	80	Slurry [29]
SBA-15	8.6	1.9	20	503	2.0	4.0	270[h]	Gas [26]
SBA-15	8.6	1.9	20	503	2.0	2.4	350[h]	Gas [26]

[a] D_{av}, average pore diameter; V_p, pore volume; Co nitrate impregnated.
[b] Ratio of catalyst amount (g) to feed gas rate (mol/h).
[c] Space–time yield of C_{10}–C_{20} fraction, estimated using CO conversion and chain growth probability.
[d] Slurry or gas means a slurry or gas phase reactor, respectively.
[e] Equimolar mixture of Co nitrate and acetate.
[f] Hexagonal mesoporous silica.
[g] Mesoporous silica with Si/Al of 19; 0.5% Ir added.
[h] Calculated using CO conversion and selectivity to C_{10}–C_{20} hydrocarbons.

STY at 503 K was as large as 260–270 g C/kg_{cat} h with the Co(10A+10N) and Co(20N) catalysts [26]. Fig. 6 also point outs that the STY or the conversion with the Co(10A+10N) is much larger than the arithmetic mean of the corresponding value observed with the Co(20A) and Co(20N). In other words, the synergistic effect exists with the performance of the Co(10A + 10N) catalyst in production of C_{10}–C_{20} hydrocarbons as well as the activity, that is, CO conversion, as mentioned earlier (Table 5).

According to the TPR measurements of the fresh Co(10A+10N) after air calcination [26], the profile was not the same as that (Fig. 5A) with the fresh Co(20N) catalyst, but it was rather close to a mixed one of the TPR spectra observed with the Co(20N) and Co(20A). In other words, Co_3O_4 and Co silicates (and/or surface CoO_x species) coexisted in the Co(10A + 10N). Since this means that the proportion of the readily reducible Co_3O_4 is smaller in the Co(10A + 10N) than the Co(20N), almost the same FT performances observed with both catalysts cannot be explained by the TPR results alone. The dispersion of metallic Co may be different between them [32]. In fact, the preliminary TEM studies after H_2 reduction at 673 K and subsequent surface passivation showed the formation of the more highly dispersed particles of metallic Co on the Co(10A + 10N) than on the Co(20N). The more fine particles on the former catalyst may account for the high performance comparable to that of the Co(20N) catalyst. To make clear the catalysis of FT synthesis by the Co(10A + 10N) should be the subject of future work.

It is of interest to compare the STY of C_{10}–C_{20} hydrocarbons among different Co catalysts supported on conventional SiO_2 and mesoporous molecular sieves. The results recently reported are summarized in Table 6, where the STY is estimated by using CO conversion and the chain growth probability (α), except the present work. Since it is well known that the STY depends strongly on the catalyst properties and the conditions of FT synthesis, these data are also provided in Table 6. Among conventional SiO_2 supports, the high STY of 210 g C/kg_{cat} h was observed for Co(10A + 10N)/SiO_2 with the pore diameter of 16 nm, and it was realized by optimizing the temperature of catalyst reduction [39].

When hexagonal mesoporous silica (HMS) with the pore diameter of 2.8 nm was used as a support of Co(15N) catalyst, as seen in Table 6, large CO conversion of about 95% was observed at 513 K, and heavy wax was mainly produced, which resulted in the low STY of C_{10}–C_{20} hydrocarbons [28]. The reasons for the high activity of the Co catalyst and the large selectivity to the wax were not clear, though they were suggested to be related to short channels and large mesoporosity of the HMS support [28]. Such a high selectivity may also be caused by large W/F of 24 g h/mol, that is, a long contact time between gas and catalyst. With the present SBA-15 support, the α on the Co(20N) catalyst increased with increasing W/F, and the STY thus showed a maximal value of 350 g C/kg_{cat} h at 2.4 g h/mol [26]. It has been reported that the α is dependent on the pore diameter of Co(20N)/SiO_2 catalyst and maximal at the moderate diameter of 10 nm [17], whereas the α tends to be higher at a larger pore diameter in the range of 2.0–7.5 nm with 5–7% Co(N) catalysts on mesoporous molecular sieves, though CO conversion is always as low as <5% [18].

Since product distribution in FT synthesis usually follows the Anderson–Schultz–Flory distribution, the STY of C_{10}–C_{20} hydrocarbons is determined by both CO conversion and chain growth provability (α). As described above, small Co particles in narrow pores may show lower reducibility but provide higher metal dispersion, whereas large Co particles in wide pores may exhibit the reverse reducibility and dispersion [17,18]. The extent of overall reduction may thus be one of the key factors for determining not only CO conversion but α. In other words, there may be the optimal pore size that can provide the highest STY of C_{10}–C_{20} fraction. It has been accepted that catalyst supports with wide pores can overcome mass transport limitations in FT synthesis to

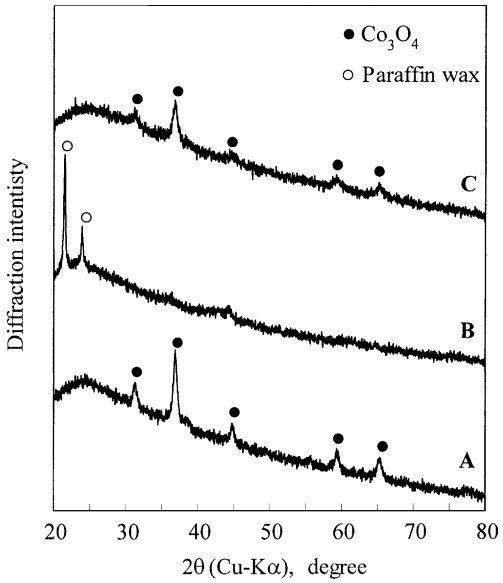

Fig. 7. XRD profiles for Co(20N)/SBA-15 catalysts under different conditions: (A) fresh catalyst after air calcination; (B) used catalyst after FT synthesis at 503 K; (C) used catalyst after re-calcination.

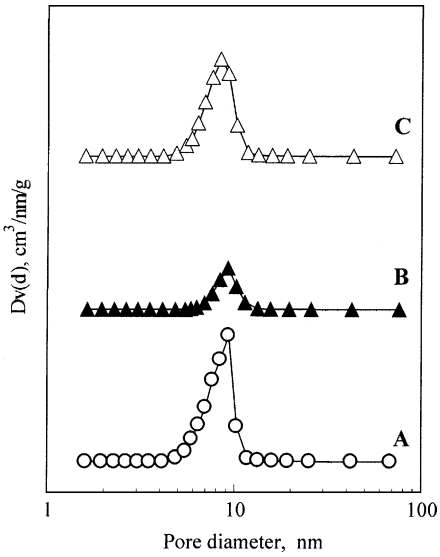

Fig. 8. Pore size distribution for Co(20N)/SBA-15 catalysts under different conditions: (A) fresh catalyst after air calcination; (B) used catalyst after FT synthesis at 503 K; (C) used catalyst after re-calcination.

some extent [9,13–17]. As a result of a complex interplay between these factors, the SBA-15 support with the diameter of 8.6 nm used in the present study may be suitable for producing C_{10}–C_{20} hydrocarbons efficiently.

3.5. Structural stability of SBA-15 supported Co catalysts

The XRD profiles for fresh and used Co(20N) catalysts are compared in Fig. 7, where the latter one is recovered after reaction at 503 K. In Fig. 7B, after the FT run, very sharp diffraction lines attributable to paraffin wax appeared, and weak XRD peaks of Co_3O_4 observed for the fresh catalyst disappeared, though any XRD signals of metallic Co could not be detected. The latter two observations may show the transformation of the initial Co_3O_4 to metallic Co particles that are too fine to be detected by XRD. The presence of the wax indicates that significant amounts of long chain paraffinic hydrocarbons are retained inside the mesopores when the catalyst is quenched for recovery. Such retention was supported by the considerable decrease in the pore volume of the used Co(20N), as will be mentioned in Fig. 8. When it was calcined again at 773 K, the XRD signals of the wax disappeared completely, and Co_3O_4 appeared again (Fig. 7C). The average crystalline size of the oxide species was estimated to be 13 nm, which was slightly smaller than that (20 nm) for the fresh Co(20N) (Table 4).

Fig. 5D also shows the TPR result for the re-calcined Co(20N). The spectrum at ≤800 K could be almost completely overlaid with that (Fig. 5A) for the fresh catalyst. This observation indicates that the reducibility of Co_3O_4 in the Co(20N) does not change significantly before and after FT synthesis, because the H_2 consumption at ≤800 K originates from the reduction of Co_3O_4 to metallic Co as mentioned above.

When the pore size distribution for fresh and used Co(20N) catalysts was compared in Fig. 8A and B, the peak height for the used catalyst was reduced to be one third of that for the fresh one. The reduction means the considerable decrease in the pore volume and must be caused by the retention of significant amounts of waxy materials inside the mesopores as indicated by the XRD peaks of paraffin wax (Fig. 7B). The re-calcination of the used Co(20N) burned the wax out (Fig. 7C) and consequently restored the pore distribution to almost the same state as with the fresh catalyst, as shown in Fig. 8C. These changes in the pore size distribution were also observed with the Co(10A + 10N) [26].

These observations thus show that not only the dispersion state of Co species in the Co(20N)/SBA-15, which exhibits the highest performance in FT synthesis at 503 K, but also the pore structure is stable. Such a structural stability may be ascribed to thicker walls of the mesopores in the SBA-15 than in other molecular sieve silica materials [21].

4. Conclusions

Cobalt catalysts supported on MCM-41 and SBA-15 with well-defined mesopores by the different methods have been studied in gas phase Fischer–Tropsch synthesis at 2.0 MPa to efficiently produce C_{10}–C_{20} hydrocarbons as the main components of diesel fuel. The conclusions are summarized as follows:

1. The method of exchanging template ions in uncalcined MCM-41 with Co^{2+} ions in an aqueous solution of Co

acetate or nitrate makes it possible to hold large amounts of 10–20% Co inside the mesopores while maintaining the structure regularity of MCM-41 to some extent, compared with the impregnation method using the calcined MCM-41.

2. The increase in Co loading from 10 to 20% for the exchanged catalysts with pore diameters of 2.7–2.9 nm enhances not only CO conversion but also selectivity to C_{10}–C_{20} fraction at 523 K, irrespective of the kind of Co precursor.
3. When an ethanol solution of Co acetate is impregnated at metal loading of 20% with four kinds of SBA-15 supports with different pore diameters, the catalyst with the moderate diameter of 8.3 nm provides the largest CO conversion at 523 K, and it is more active than MCM-41 supported Co catalysts.
4. In FT synthesis at 503 K, the acetate-derived Co on the SBA-15 is almost inactive even at loading of 20%, but contrarily, the catalyst prepared from Co nitrate alone or an equimolar mixture of the acetate and nitrate provides high CO conversion of 85–90% and achieves large space–time yield of 260–270 g C/kg_{cat} h for C_{10}–C_{20} hydrocarbons.
5. Since the temperature-programmed reduction measurements of fresh Co/SBA-15 catalysts after air calcination reveal that the acetate is transformed to less reducible Co silicates, whereas the nitrate-derived catalyst exists mainly as readily reducible Co_3O_4, such differences can account for the quite distinct catalytic activity observed at 503 K with the two precursors.
6. The X-ray diffraction, N_2 adsorption, temperature-programmed reduction measurements after FT synthesis and subsequent air calcination strongly suggest that the most effective Co/SBA-15 catalyst is stable in not only the dispersion and reducibility of the oxide species but the mesoporous structure.

Acknowledgements

The present work was supported by Research for the Future Program of Japan Society for the Promotion of Science (JSPS) under the Project “Synthesis of Ecological High Quality Transportation Fuels” (JSPS-RFTF98P01001).

References

[1] L. Xu, S. Bao, R.J. O’Brien, A. Raje, B.H. Davis, CHEMTECH (1998) 47.
[2] H. Schulz, Appl. Catal. A 186 (1999) 3.
[3] B.H. Davis, Fuel Process. Technol. 71 (2001) 157.
[4] T. Wakatsuki, Y. Morita, H. Okado, K. Inaba, H. Hirayama, M. Shimura, K. Kawazuishi, O. Iwamoto, T. Suzuki, Stud. Surf. Sci. Catal. 136 (2001) 117.
[5] E. Iglesia, Preprints, ACS Div. Fuel. Chem. 47 (2002) 128.
[6] M.E. Dry, Catal. Today 71 (2002) 227.
[7] M. Yamada, Energy and Fuels 17 (2003) 797.
[8] G.A. Mills, Fuel 73 (1994) 1243.
[9] E. Iglesia, Appl. Catal. A 161 (1997) 59.
[10] P.J. van Berge, R.C. Everson, Stud. Surf. Sci. Catal. 107 (1997) 207.
[11] G.P. van der Laan, A.A.C.M. Beenackers, Catal. Rev. Sci. Eng. 41 (1999) 255.
[12] R. Zennaro, M. Tagliabue, C.H. Bartholomew, Catal. Today 58 (2000) 309.
[13] R.C. Reuel, C.H. Bartholomew, J. Catal. 85 (1984) 78.
[14] D. Vanhove, Z. Zhuyong, L. Makambo, M. Blanchard, Appl. Catal. 9 (1984) 327.
[15] E. Iglesia, S.L. Soled, R.A. Fiato, J. Catal. 137 (1992) 212.
[16] K. Fujimoto, M. Shimose, Y.Z. Han, Stud. Surf. Sci. Catal. 107 (1997) 181.
[17] A.A. Saib, M. Claeys, E. van Steen, Catal. Today 71 (2002) 395.
[18] A.Y. Khodakov, A. Griboval-Constant, R. Bechara, V.L. Zholobenko, J. Catal. 206 (2002) 230.
[19] C.T. Kresge, M.E. Leonowicz, W.J. Roth, J.C. Vartuli, J.S. Beck, Nature 359 (1992) 710.
[20] S. Inagaki, Y. Fukushima, K. Kuroda, J. Chem. Soc., Chem. Commun. (1993) 680.
[21] E. Zhao, J. Feng, Q. Huo, N. Melosh, G.H. Fredrickson, B.F. Chmelka, G.D. Stucky, Science 279 (1998) 548.
[22] A. Corma, Chem. Rev. 97 (1997) 2373.
[23] Y. Wang, M. Noguchi, Y. Takahashi, Y. Ohtsuka, Catal. Today 68 (2001) 4.
[24] Y. Wang, Y. Takahashi, M. Noguchi, Y. Ohtsuka, in: Proceedings of the Seventh China-Japan Symposium on Coal and C_1 Chemistry, Hainan Island, China, 2001, pp. 65–68.
[25] N.K. Mal, Y. Ohtsuka, in: Proceedings of the Fourth Tokyo Conference of Advanced Catalytic Science and Technology, Tokyo, 2002, p. 336.
[26] Y. Ohtsuka, T. Arai, S. Takasaki, N. Tsubouchi, Energy and Fuels 17 (2003) 804.
[27] T. Iwasaki, M. Reinikainen, Y. Onodera, H. Hayashi, T. Ebina, T. Nagase, K. Torii, K. Kataja, A. Chatterjee, Appl. Surf. Sci. 130 (1998) 845.
[28] D. Yin, W. Li, H. Xiang, Y. Sun, B. Zhong, S. Peng, Microporous Mesoporous Mater. 47 (2001) 15.
[29] K. Okabe, M. Wei, H. Arakawa, Energy and Fuels 17 (2003) 822.
[30] J.S. Beck, J.C. Vartuli, W.J. Roth, M.E. Leonowicz, C.T. Kresge, K.D. Schmitt, C.T.W. Cu, D.H. Olson, E.W. Sheppard, S.B. McCullen, J.B. Higgins, J.L. Schlenker, J. Am. Chem. Soc. 114 (1992) 10834.
[31] M. Yonemitsu, Y. Tanaka, M. Iwamoto, J. Catal. 178 (1998) 207.
[32] S. Sun, N. Tsubaki, K. Fujimoto, Appl. Catal. A 202 (2000) 121.
[33] E. Iglesia, S.L. Soled, R.A. Fiato, G.H. Via, J. Catal. 143 (1993) 345.
[34] N. Tsubaki, S. Sun, K. Fujimoto, J. Catal. 199 (2001) 236.
[35] M.P. Rosynek, C.A. Polansky, Appl. Catal. 73 (1991) 97.
[36] I. Puskas, T.H. Fleisch, J.B. Hall, B.L. Meyers, R.T. Rochinski, J. Catal. 134 (1992) 615.
[37] H. Ming, B.G. Baker, Appl. Catal. A 123 (1995) 23.
[38] E. van Steen, G.S. Sewell, R.A. Makhothe, G. Micklethwaite, H. Manstein, M. de Lange, C.T. O’Connor, J. Catal. 162 (1996) 220.
[39] G. Bian, T. Mochizuki, N. Fujishita, H. Nomoto, M. Yamada, Energy and Fuels 17 (2003) 799.